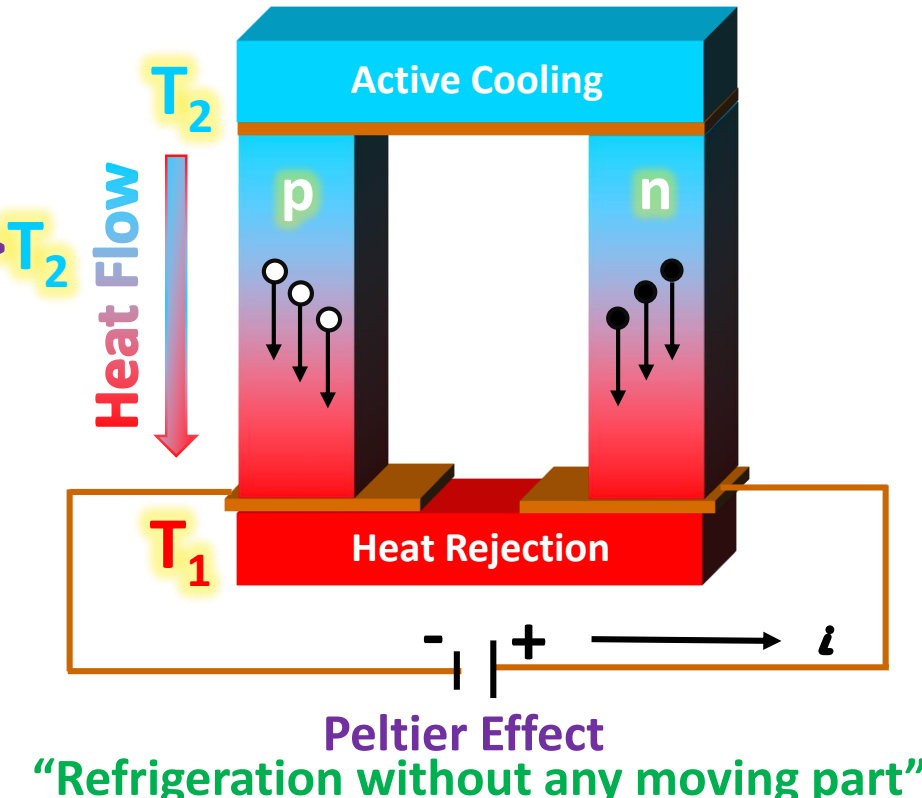
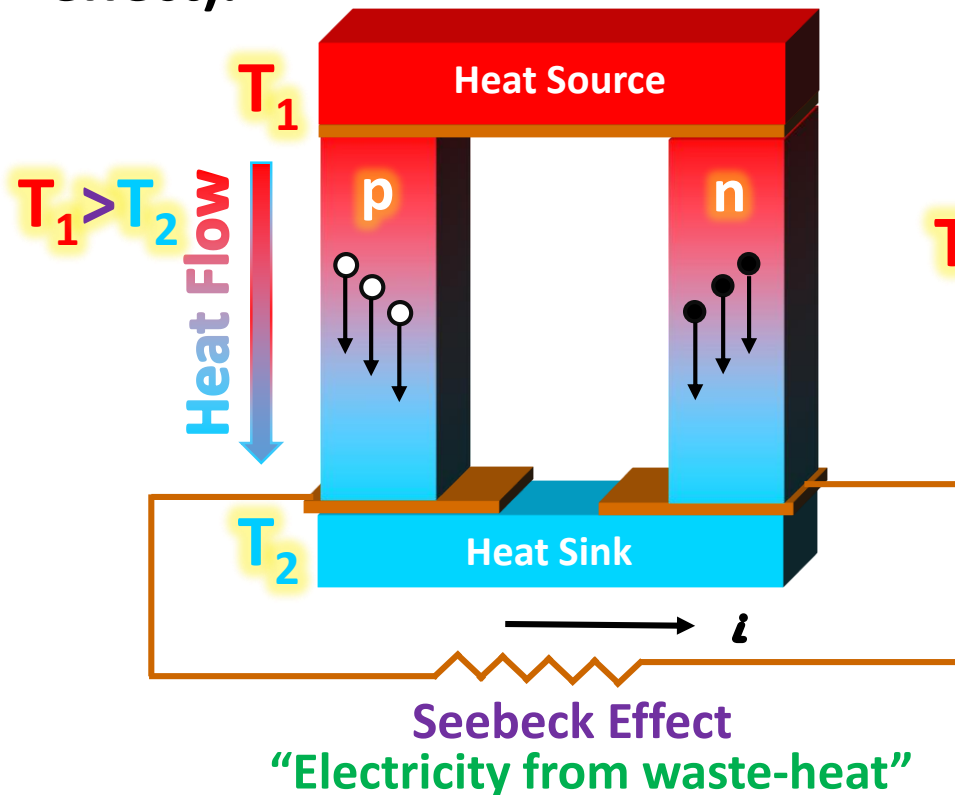


Computational Exploration of Ultralow Lattice Thermal Conductivity and High Figure of Merit in p-type Bulk RbX_2Sb ($\text{X}=\text{K, Na}$)

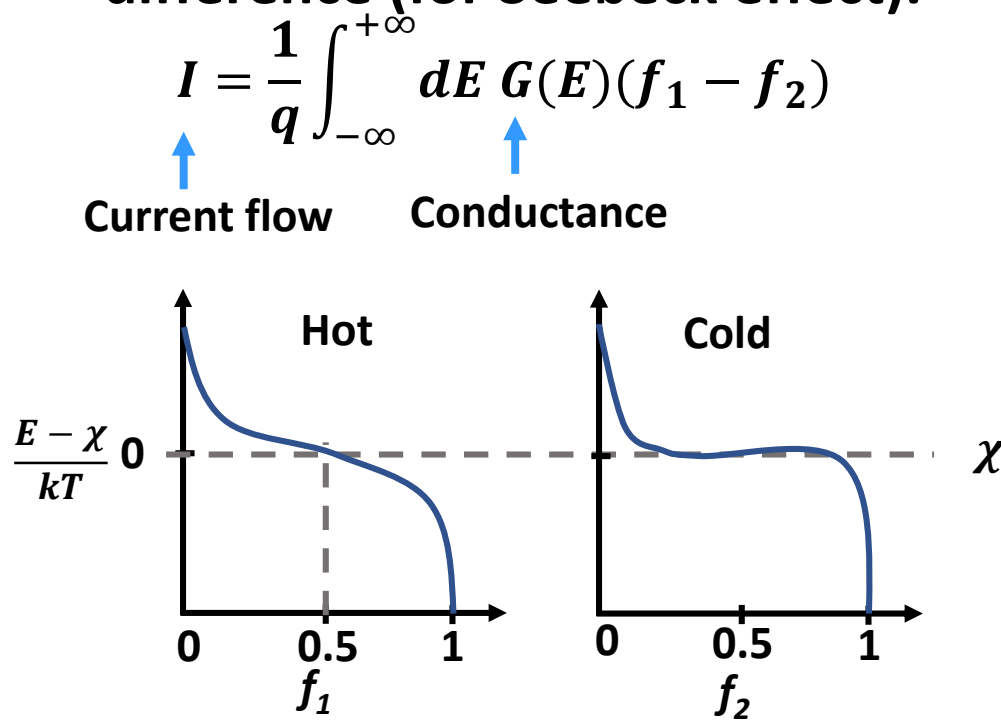
What are thermoelectric materials?

- Materials that generate electricity due to temperature difference(Seebeck effect) or flow of electricity through which result temperature difference(Peltier effect).



What are thermoelectric materials? (contd.)

- Electricity flows due to voltage difference and voltage difference comes from the difference in electrochemical potential.
- In thermoelectric materials the voltage difference comes from the temperature difference (for Seebeck effect).



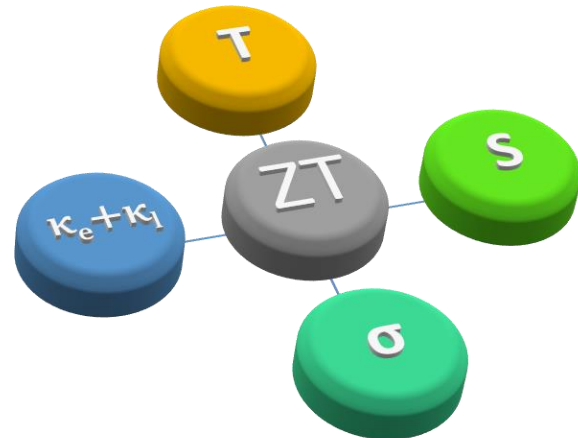
$$f_i = \frac{1}{1 + e^{\frac{(E - \chi_i)}{kT_i}}}$$

↑ Fermi function ↑ Electrochemical potential

Why we are interested in thermoelectric materials?

- Major cause of global warming is the waste heat.
- Almost 75% of the energy produced by the mankind are squandered as waste heat.
- The waste heat can be used as the renewable energy source for the generation of electricity by the aid of the Seebeck effect of thermoelectric materials.

Figure of merits



Seebeck Coefficient Electrical conductivity

$$ZT = \frac{S^2 \sigma T}{\kappa_e + \kappa_l}$$

Absolute Temperature
Lattice Thermal Conductivity
Electrical Thermal Conductivity

Figure of merit

$$S = \frac{\Delta V}{\Delta T}$$

ability to generate voltage difference due to unit temperature difference

Interdependencies of the parameters

$$S(T, \chi) = \frac{\int_{-\infty}^{\infty} dE \left(-\frac{\partial f(E, T, \chi)}{\partial E} \right) \sigma(E) (E - \chi)}{qT \int_{-\infty}^{\infty} dE \left(-\frac{\partial f(E, T, \chi)}{\partial E} \right) \sigma(E)} \quad \dots(1)$$

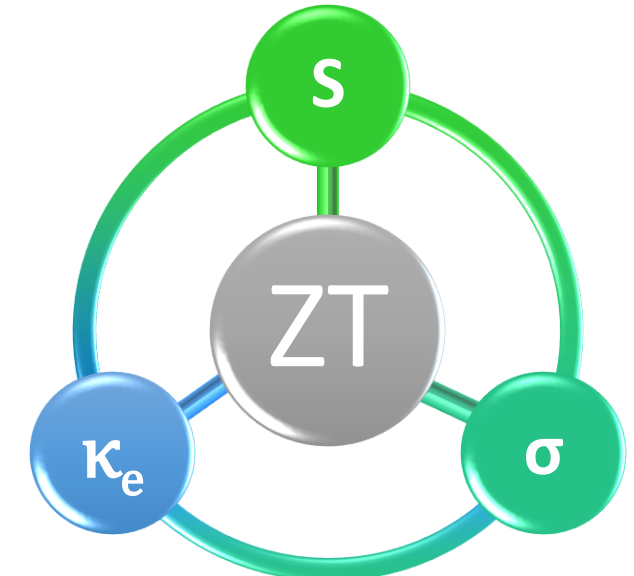
Energy Electrochemical potential
↓ ↓

$$\sigma(T, \chi) = \int_{-\infty}^{\infty} dE \left(-\frac{\partial f(E, T, \chi)}{\partial E} \right) \sigma(E) \quad \dots(2)$$
$$\kappa_e = \kappa_0 - T \sigma S^2 = L \sigma T \quad \dots(3)$$

↑
Lorenz Constant

$f(E, T, \chi)$ ← Fermi function.

κ_0 ← Electrical thermal conductivity under closed circuit condition.



Contradictory relations between the parameters

$$S = \frac{2k_B^2 T}{3e\hbar^2} \left(\frac{\pi}{3n}\right)^{2/3} m_d^*, \quad \text{where } m_d^* \propto m_b^* = \frac{\hbar^2}{d^2 E_{edge}} \frac{dk^2}{\text{band effective mass}}$$

Charge carrier concentration DOS effective mass band effective mass

$$\sigma = \frac{ne^2\tau}{m_b^*} = ne\mu, \text{ where } \tau = \frac{m_b^*\mu}{e}$$

Charge carrier mobility Charge carrier relaxation time

$$\kappa_e = \kappa_0 - T\sigma S^2 = L\sigma T$$

$$ZT = \frac{S^2 \sigma T}{\kappa_e + \kappa_l}$$



Metal
High electrical conductivity

+



Semiconductor
High Seebeck coefficient

+



Glass
Low thermal conductivity

=>

Good thermoelectric material

Our present work with bi-alkali antimonides

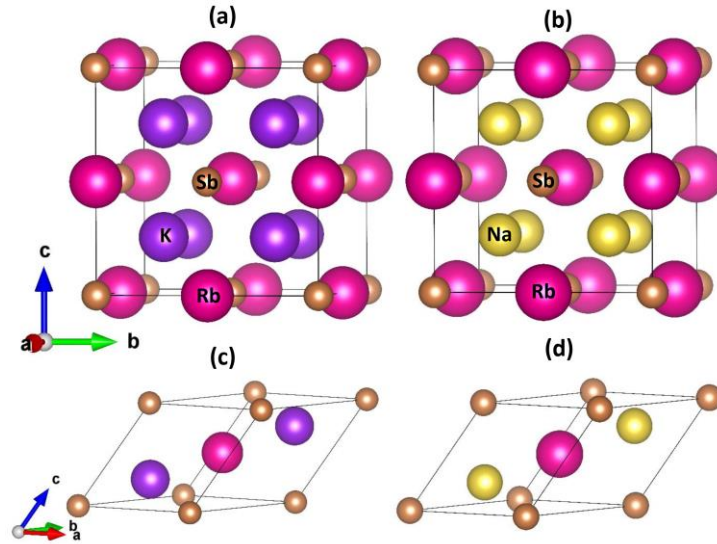


Figure 1: Conventional unit cells (a), (b) and primitive unit cells (c), (d) of RbK_2Sb and RbNa_2Sb , respectively

- ❖ Cubic crystal structure with space group Fm-3m (No. 225)
- ❖ 16 atoms per conventional unit cell
- ❖ 4 atoms per primitive unit cell

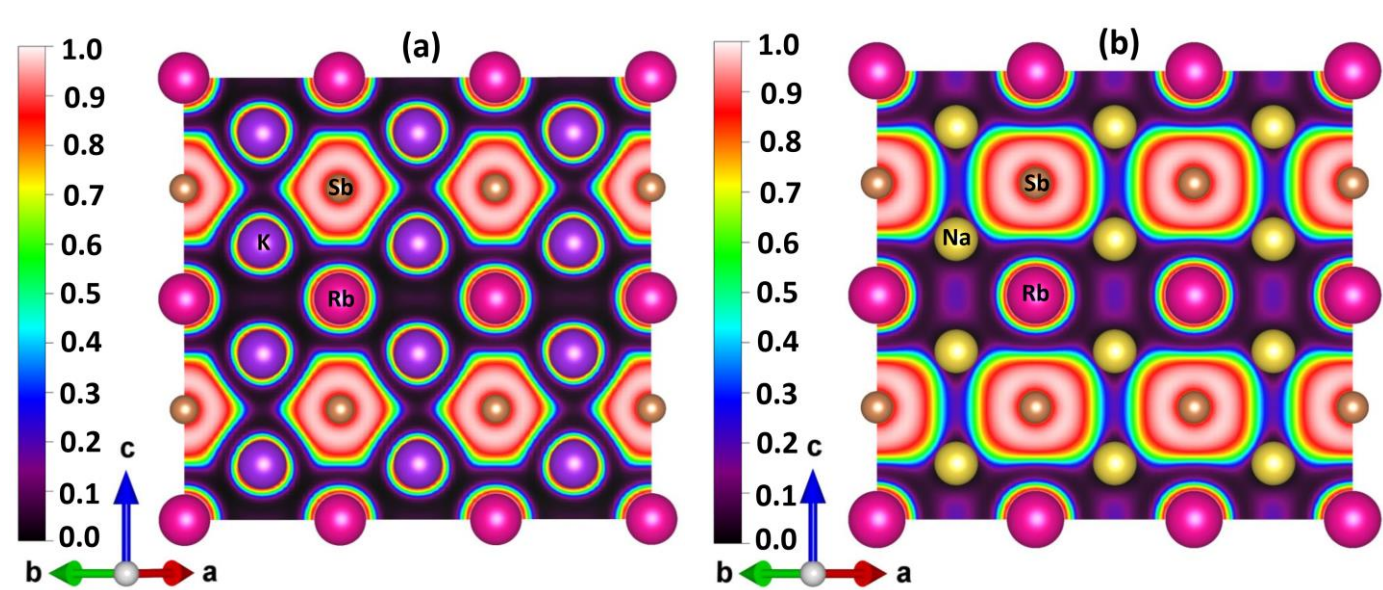


Figure 2: Electron localization function plot along the (110) plane of (a) RbK_2Sb and (b) RbNa_2Sb .

From Figure 2:

- ❖ Negligible ELF values between the atom pairs for both systems
- ❖ Electrons are tightly bound to the atoms resulting in very poor overlaps between the atom pairs
- ❖ Represent ionic characteristic of the bonds in both the systems

Stability of the systems

- ❖ Negative formation energy (-0.41 and -0.44 eV/atom for RbK₂Sb and RbNa₂Sb, respectively): Thermodynamically stable
- ❖ Thermally stable from ab Initio molecular dynamics simulation at 700 K

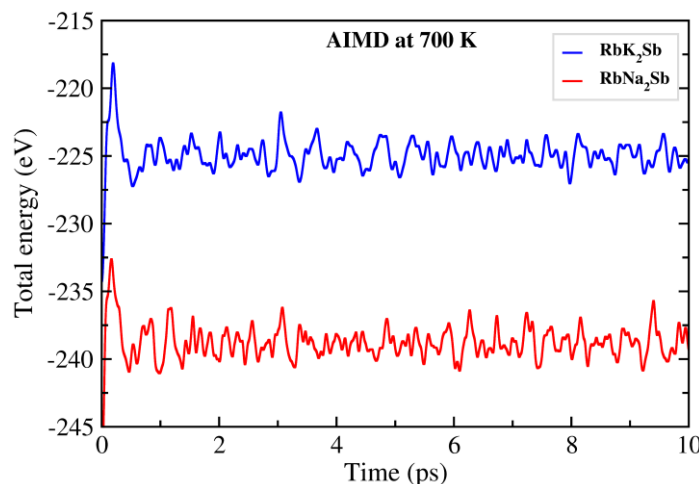


Figure 3: AIMD plot at 700 K up to 10 ps

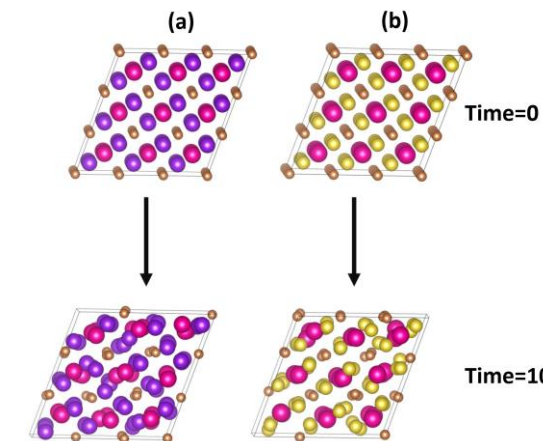


Figure 4: Structures of (a) RbK₂Sb and (b) RbNa₂Sb after 10 ps of AIMD simulation.

- ❖ Satisfies the Born stability criteria in terms of elastic stiffness constants: Mechanically stable
- ❑ Born criteria for cubic systems: $C_{11}-C_{12}>0$, $C_{11}+2C_{12}>0$ and $C_{44}>0$

Stability of the systems (contd.)

❖ Non-negative phonon frequencies: Dynamically stable

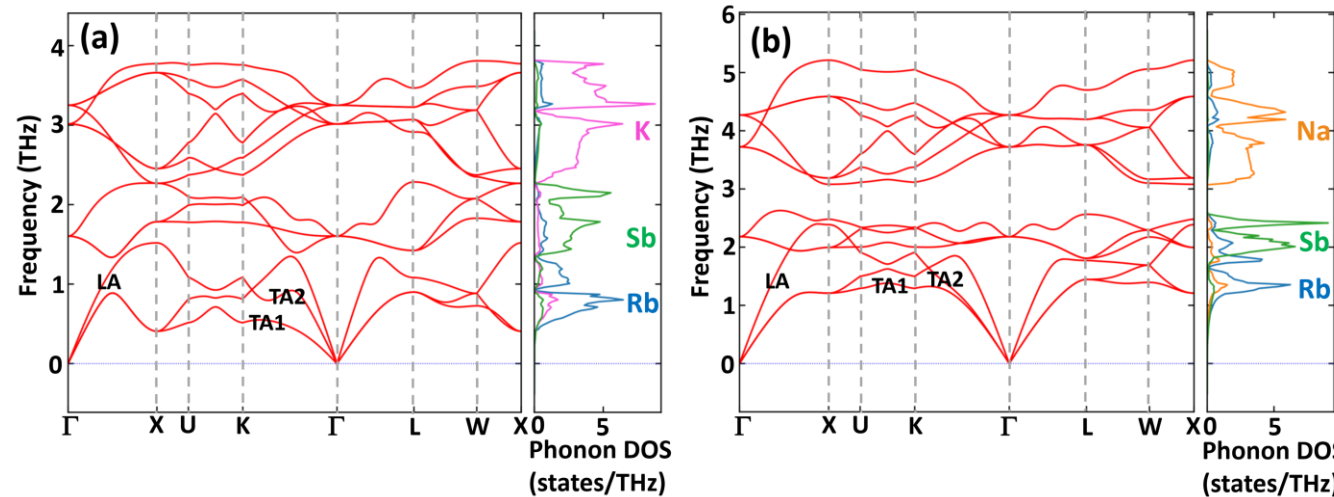


Figure 5: Phonon dispersion and phonon density of state of (a) RbK_2Sb , (b) RbNa_2Sb

- 4 atoms per primitive unit cell
- $3 \times 4 = 12$ degrees of freedom: 12 phonon modes = 3 acoustic ($2\text{TA} + 1\text{LA}$) + 9 optical (3 low frequency + 6 high frequency)
- $M_K > M_{\text{Na}}$: $\omega(\text{RbK}_2\text{Sb}) < \omega(\text{RbNa}_2\text{Sb})$
- Avoided crossing in RbK_2Sb phonon dispersion.
- Flattening of the acoustic bands of the RbK_2Sb
- In RbNa_2Sb : low frequency optical and acoustic bands overlap

Electronic structure

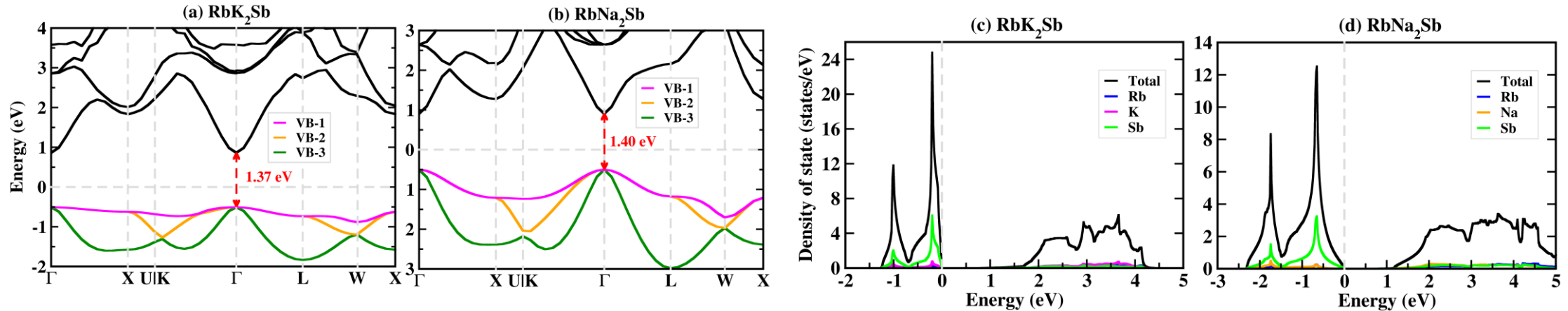
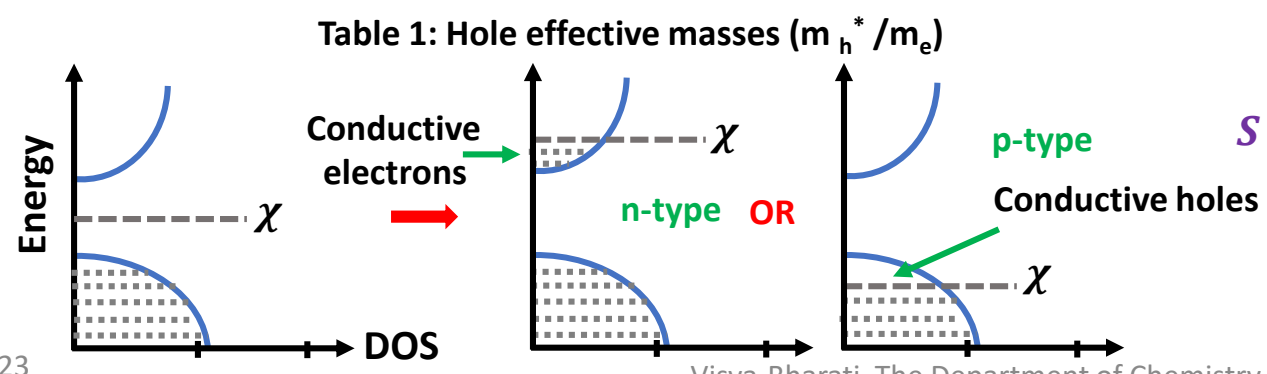


Figure 6: Electronic band structure using HSE06 functional: (a) RbK_2Sb , (b) RbNa_2Sb and electronic DOS: (c) RbK_2Sb , (d) RbNa_2Sb

| Systems | VB-1 | | | VB-2 | | | VB-3 | | | Systems | CB | | |
|--------------------------|------------------------|------------------------|------------------------|------------------------|------------------------|------------------------|------------------------|------------------------|------------------------|--------------------------|------------------------|------------------------|------------------------|
| | $\Gamma \rightarrow X$ | $\Gamma \rightarrow K$ | $\Gamma \rightarrow L$ | $\Gamma \rightarrow X$ | $\Gamma \rightarrow K$ | $\Gamma \rightarrow L$ | $\Gamma \rightarrow X$ | $\Gamma \rightarrow K$ | $\Gamma \rightarrow L$ | | $\Gamma \rightarrow X$ | $\Gamma \rightarrow K$ | $\Gamma \rightarrow L$ |
| RbK_2Sb | -9.830 | -8.780 | -2.442 | -9.830 | -1.826 | -2.442 | -0.156 | -0.169 | -0.161 | RbK_2Sb | 0.136 | 0.136 | 0.128 |
| RbNa_2Sb | -0.856 | -0.907 | -0.877 | -0.856 | -0.830 | -0.877 | -0.112 | -0.114 | -0.104 | RbNa_2Sb | 0.113 | 0.117 | 0.107 |



Thermoelectric properties

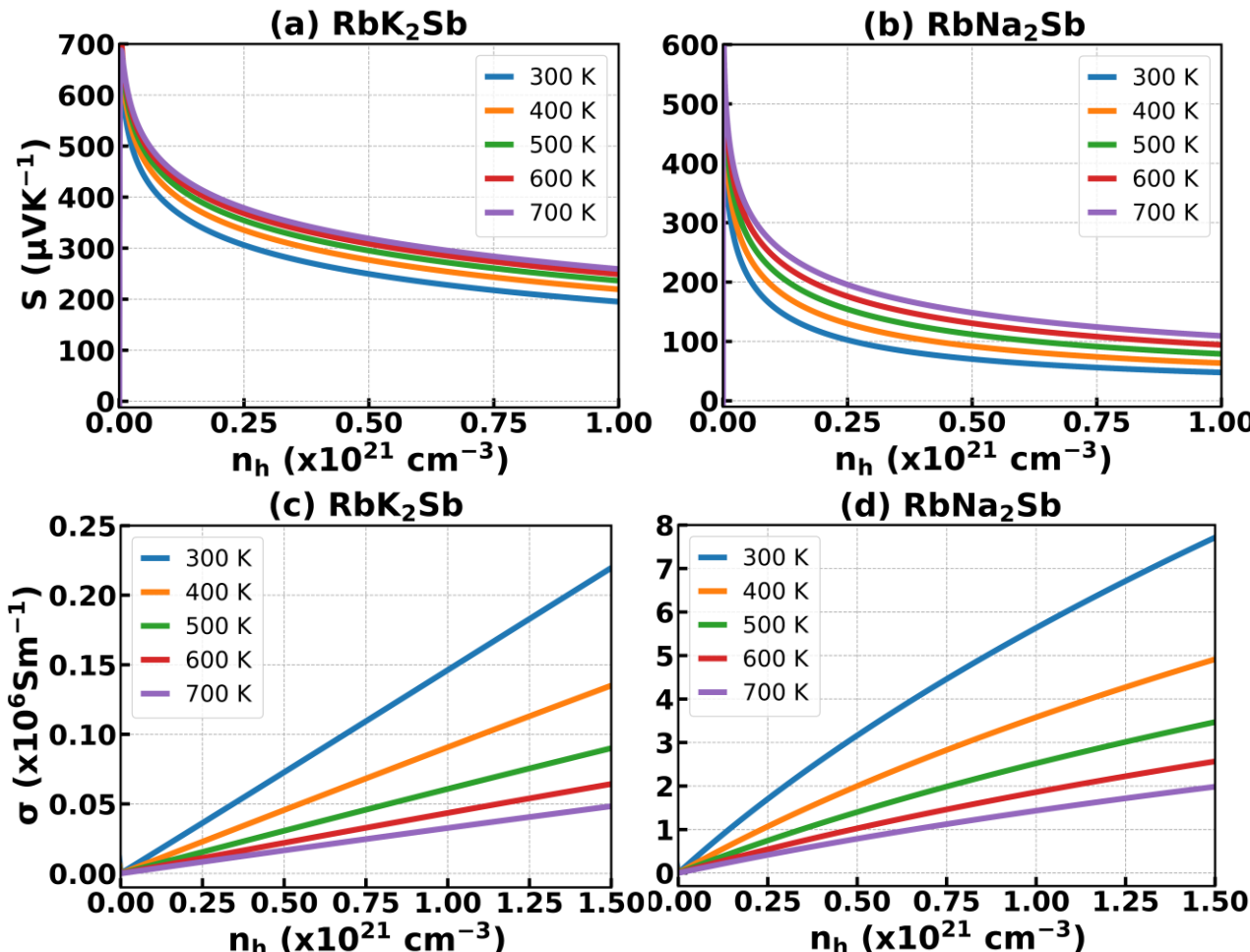


Figure 7: Seebeck coefficient of p-type (a) RbK₂Sb, (b) RbNa₂Sb and electrical conductivity of p-type (c) RbK₂Sb, (d) RbNa₂Sb as a function of hole concentration

| Temperature (K) | RbK ₂ Sb | | RbNa ₂ Sb | |
|-----------------|--------------------------------|-------------|--------------------------------|-------------|
| | μ ($cm^2 V^{-1} s^{-1}$) | τ (fs) | μ ($cm^2 V^{-1} s^{-1}$) | τ (fs) |
| 300 | 2.28 | 12.8 | 451.38 | 220 |
| 400 | 1.48 | 8.3 | 291.35 | 142 |
| 500 | 1.05 | 5.9 | 209.28 | 102 |
| 600 | 0.80 | 4.5 | 157.98 | 77 |
| 700 | 0.64 | 3.6 | 125.15 | 61 |

Table 3: Hole mobilities and relaxation times

$$S = \frac{2k_B T}{3e\hbar^2} \left(\frac{\pi}{3n}\right)^{2/3} m_d^*, \text{ where } m_d^* \propto m_b^*$$

$$\sigma = \frac{ne^2 \tau}{m_b^*} = \frac{ne^2 \mu}{e}, \text{ where } \tau = \frac{m_b^* \mu}{e}$$

$$\kappa_e \propto \sigma$$

Thermoelectric properties (contd.)

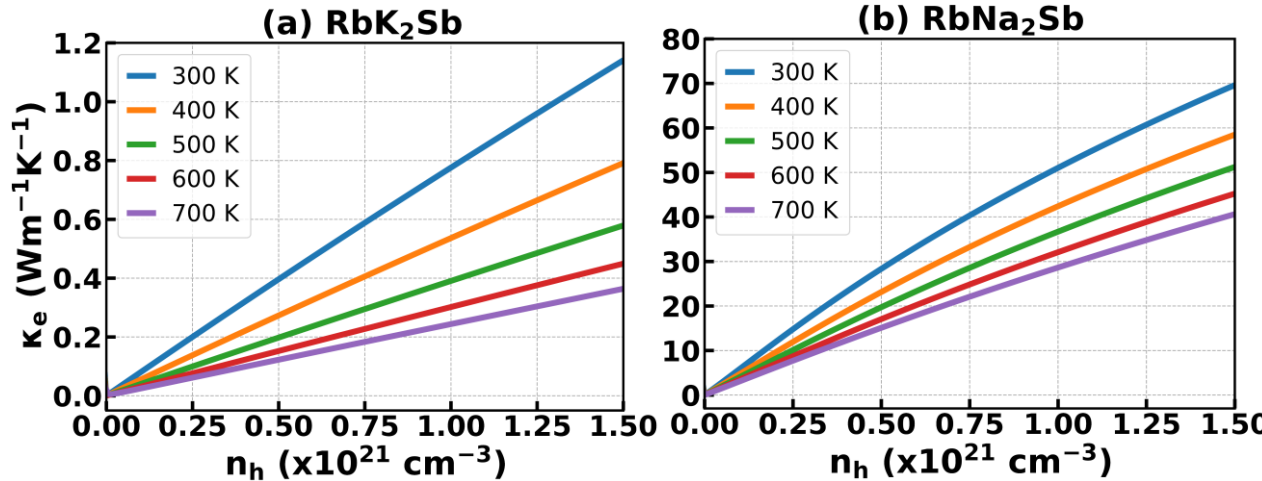


Figure 8: Electronic thermal conductivity of p-type (a) RbK₂Sb, (b) RbNa₂Sb as function of hole concentration

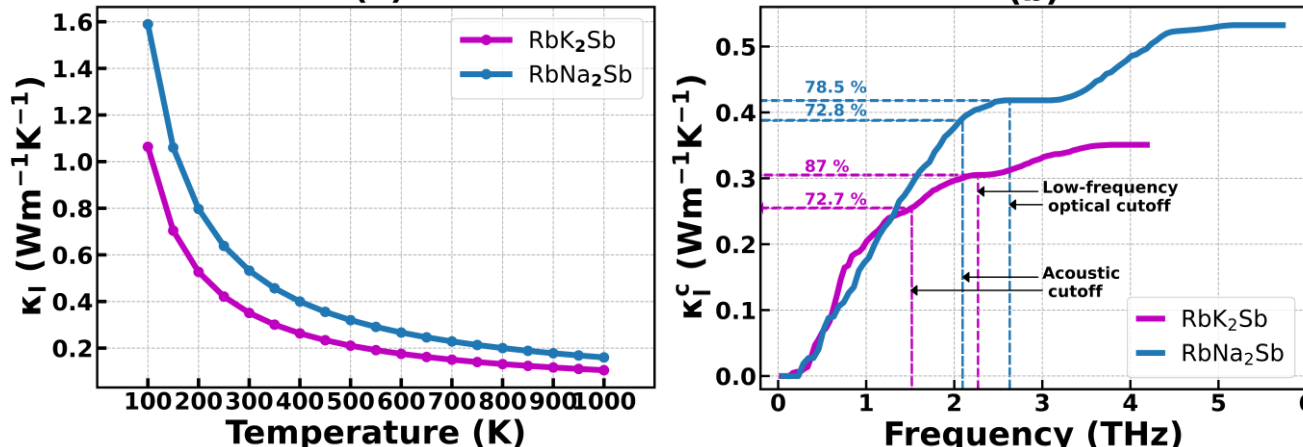


Figure 9: (a) Lattice thermal conductivity as function of temperature
(b) Cumulative lattice thermal conductivity as function of frequency

$$\kappa_e \propto \sigma$$

$$ZT = \frac{S^2 \sigma T}{\kappa_e + \kappa_l}$$

Lattice thermal conductivity Specific heat at constant volume

$$\kappa_l(T) = \frac{1}{3} \langle \tau \rangle \langle v_g^2 \rangle C_v(T)$$

Average relaxation time Mean square group velocity

| Systems | 300 K | 400 K | 500 K | 600 K | 700 K |
|----------------------|---------|---------|---------|---------|---------|
| RbK ₂ Sb | 0.35087 | 0.26307 | 0.21044 | 0.17536 | 0.15031 |
| RbNa ₂ Sb | 0.53243 | 0.39974 | 0.31997 | 0.26673 | 0.22868 |

Table 5: Lattice thermal conductivities at different temperatures

Cumulative lattice thermal conductivity Mode specific phonon frequency

$$\kappa_l^c(\omega) = \int_0^\omega \frac{1}{N} \sum_s \kappa_{l,s} \delta(\omega_s - \omega') d\omega'$$

Contribution to lattice thermal conductivity from phonon mode s

Thermoelectric properties (contd.)

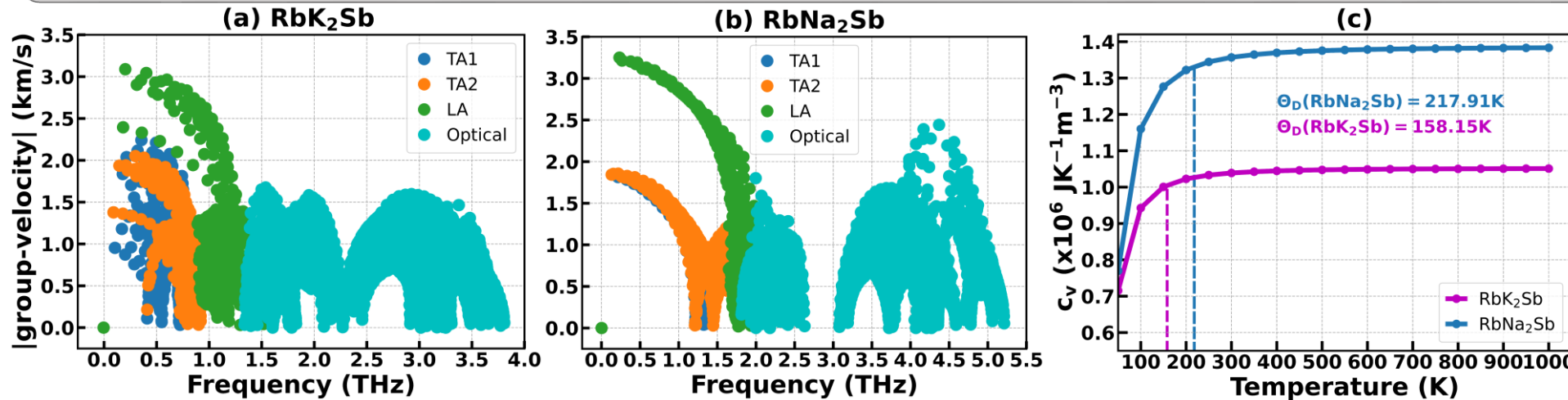


Figure 10: Mode specific group velocity as a function of phonon frequency for
 (a) RbK₂Sb, (b) RbNa₂Sb. (c) Specific heat at constant volume as a function of temperature

| Systems | $v_{g,LA}$ (km/s) | $v_{g,TA1}$ (km/s) | $v_{g,TA2}$ (km/s) |
|----------------------|-------------------|--------------------|--------------------|
| RbK ₂ Sb | 3.08 | 2.24 | 2.05 |
| RbNa ₂ Sb | 3.25 | 1.85 | 1.86 |

Table 6: Maximum mode specific group velocities at the vicinity of the Γ -point

Comparable and even lower than many TE materials reported earlier like 2D α -Te (>4 km/s), $Ti_{3-x}Mo_xC_2T_2$ (x=0.5,1,1.5,2.5,2.5, T=-OH/-O/-F)(>6 km/s), 2D BP/MoS₂ vdW hetero-bilayer(>12 km/s) etc.

Debye temperature is the Temperature of the crystal's Highest normal vibrational mode, i.e., above Θ_D all the phonons get excited.

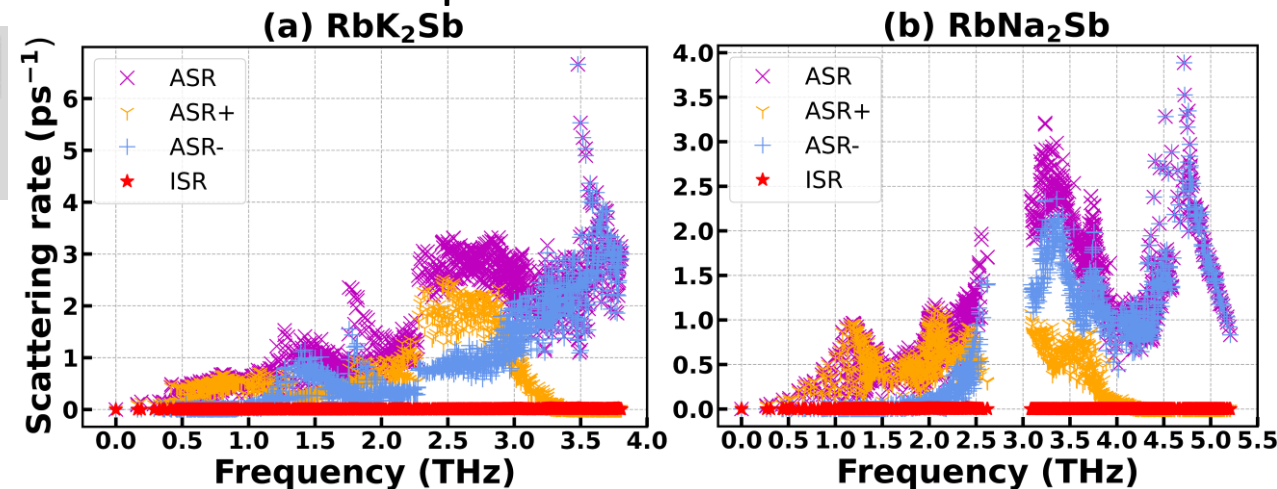


Figure 11: Scattering rates as functions of phonon frequency for (a) RbK₂Sb, (b) RbNa₂Sb

Thermoelectric properties (contd.)

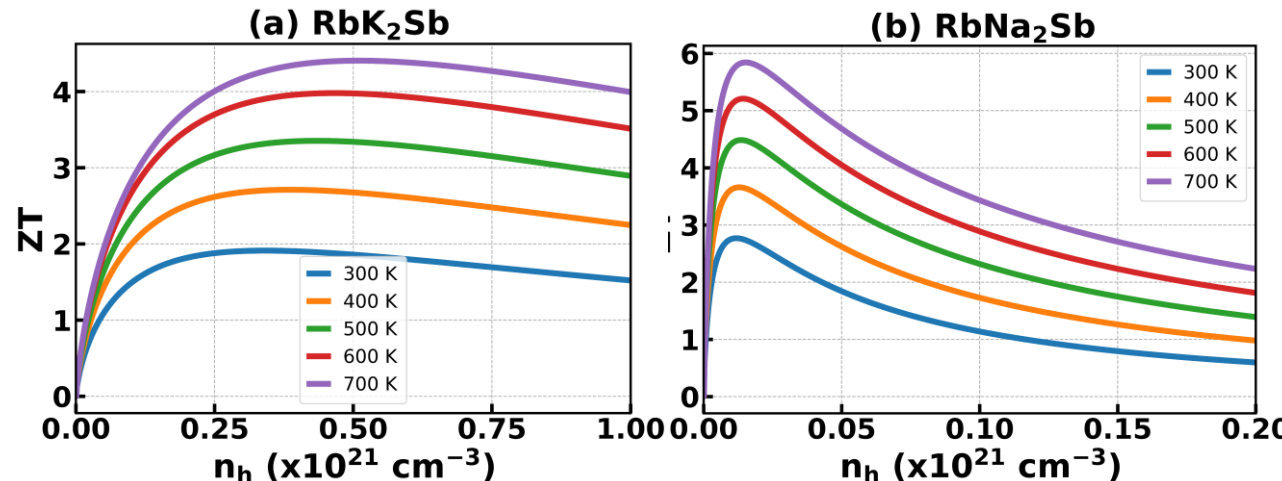


Figure 12: ZT as function of hole concentration at the temperature range 300-700 K for (a) RbK₂Sb, (b) RbNa₂Sb

(ZT)_{max} for other full-Heusler compounds reported earlier:

- n- and p-type Ba₂AuBi shows ZT as high as 5 and 2 at 800 K [1]
- Predicted ZT for n-type Sr₂BiAu is 4.9 at 700 K [2]
- Predicted ZT for n-type Sr₂SbAu is 3.4 at 750 K [2]
- ZT for n-type Sr₂AsAu is 3.3 at 700 K [3]

| Systems | 300 K | 400 K | 500 K | 600 K | 700 K |
|----------------------|-------|-------|-------|-------|-------|
| RbK ₂ Sb | 1.91 | 2.71 | 3.35 | 3.97 | 4.40 |
| RbNa ₂ Sb | 2.76 | 3.65 | 4.48 | 5.20 | 5.84 |

Table 7: (ZT)_{max} for p-type RbK₂Sb and RbNa₂Sb at the temperature range 300-700 K

Conclusion:

The bi-alkali antimonides, we have studied can be considered as better thermoelectric materials as compared to the other full-Heusler compounds

References and acknowledgments

References:

- [1] Park, J.; Xia, Y.; Ozoliņš, V. High Thermoelectric Power Factor and Efficiency from a Highly Dispersive Band in Ba₂BiAu. *Phys. Rev. Appl.* **2019**, *11*, 014058.
- [2] Park, J.; Xia, Y.; Ganose, A. M.; Jain, A.; Ozoliņš, V. High Thermoelectric Performance and Defect Energetics of Multipocketed Full-Heusler Compounds. *Phys. Rev. Appl.* **2020**, *14*, 024064.
- [3] Wang, W.; Dai, Z.; Wang, X.; Zhong, Q.; Zhao, Y.; Meng, S. Low Lattice Thermal Conductivity and High Figure of Merit in n-type Doped Full-Heusler Compounds X₂YAu (X= Sr, Ba; Y= As, Sb). *Int. J. Energy Res.* **2021**, *45*, 20949-20958.

Acknowledgements: We sincerely acknowledge the financial supports from CSIR (HRDG), Government of India [sanction no.01(3086)/21/EMR-II]. We also sincerely acknowledge the financial supports from UGC-BSR Mid-Career, Government of India [sanction no. F.19-257/2021(BSR)]. Myself sincerely acknowledge CSIR (HRDG), Government of India for providing me the JRF NET fellowship [sanction no. 09/202(0114)/2020-EMR-I].

THANK YOU